of the numerical computations. Values of the membrane surface charge densities and of the displacement and conduction currents permit a detailed understanding of the capacitive processes in a cell exposed to an external field. Biological implications of the TMP and cytoplasm electric fields are not clear at this time, because of a lack of relevant experimental data.

REFERENCES

[1] T. W. Dawson, M. A. Stuchly, and R. Kavet, "Electric fields in the human body due to electrostatic discharges," *IEEE Trans. Biomed. Eng.*, pp. 1460–1468, Aug.. 2004.

[2] M. Angeli and E. Cardelli, "Numerical modeling of electromagnetic fields generated by electrostatic discharges," *IEEE Trans. Magn.*, vol. 33, pp. 2199–2202, Mar. 1997.

[3] I. K. Nordenson, K. H. Mild, S. Nordstrom, A. Swein, and E. Birke, "Clastrogenic effects in human lymphocytes of power frequency electric fields: *In vivo* and *in vitro* studies," *Radiat. Environ. Biophys.*, vol. 23, pp. 191–2001, 1984.

[4] I. Nordenson, K. H. Mild, U. Ostman, and H. Ljungberg, "Chromosomal effects in lymphocytes of 400 kV-substation workers," *Radiat. Environ. Biophys.*, vol. 27, pp. 39–47, 1988.

[5] R. Kavet, L. E. Zaffanella, J. P. Dagle, and K. Ebi, "The possible role of contact currents in cancer risk associated with residential magnetic fields," *Bioelectromagnetics*, vol. 21, pp. 538–553, 2000.

[6] J. Malmivuo and R. Plonsey, *Bioelectromagnetism*. New York: Oxford Univ. Press, 1995.

[7] J. P. Reilly, *Electrical Stimulation and Electropathology*. New York: Cambridge Univ. Press.

[8] J. A. Nyenhuis, J. D. Bourland, A. V. Kildishev, and D. J. Schaefer, "Health effects and say of intense MRI gradient fields," in *Magnetic Resonance Procedures: Health Effects and Safety*, 1st ed, F. G Shellock, Ed. Cleveland, OH: CRC Press, 2001, pp. 31–52.

[9] J. A. D. Boer, J. D. Bourland, J. A. Nyenhus, C. L. G. Ham, J. M. L. Engels, F. X. Hebrank, G. Frese, and D. J. Schaefer, "Comparison of the threshold for peripheral nerve stimulation during gradient switching in whole body MR systems," *J. Magn. Reson. Imag.*, vol. 15, pp. 520–525, 2002.

[10] *C95.6TM IEEE Standard for Safety Levels with Respect to Human Exposure to Electromagnetic Fields, 0–3 kHz*, Oct. 23, 2002.

[11] T. Kotnik and D. Miklavci, "Second-order model of membrane electric field induced by alternating externaleElectric fields," *IEEE Trans. Biomed. Eng.*, vol. 47, pp. 1074–1081, Aug. 2000.

[12] P. So, K. Caputa, and M. A. Stuchly, "Peripheral nerve stimulation by gradient switching fields in MRI," in *Proc. 25th Int. EMBS Conf.*, Cancun, Mexico, Sept. 17–21, 2003.

[13] A. V. Oppenheim and R. Schafer, *Digital Signal Processing*. Englewood Cliffs, NJ: Prentice-Hall, 1975.

A Novel Algorithm to Estimate the Pulse Pressure Variation Index ΔPP

Mateo Aboy*, James McNames, Tran Thong, Charles R. Phillips, Miles S. Ellenby, and Brahm Goldstein

***Abstract*—We designed a new methodology to estimate the pulse pressure variation index (ΔPP) in arterial blood pressure (ABP). The method uses automatic detection algorithms, kernel smoothing, and rank-order filters to continuously estimate ΔPP. The technique can be used to estimate ΔPP from ABP alone, eliminating the need for simultaneously acquiring airway pressure.**

***Index Terms*—Cardiac index (CI), fluid responsiveness, pulse pressure variation (ΔPP), respiratory changes in systolic pressure, volume expansion (VE).**

I. INTRODUCTION

In this paper, we describe a methodology to estimate the pulse pressure variation index (ΔPP) in arterial blood pressure (ABP) signals. Several studies have shown ΔPP to have important clinical utility [1]–[3]. In mechanically ventilated patients, ΔPP has been found to be a potentially useful dynamic indicator of fluid responsiveness. In a study involving 40 mechanically ventilated patients with acute circulatory failure related to sepsis it was concluded that ΔPP was a sensitive and specific method for predicting and assessing the hemodynamic effects of volume expansion (VE) [4]. A review study of the indexes used in intensive care to predict fluid responsiveness found ΔPP to be one of the most specific and sensitive predictors of fluid responsiveness in sedated patients receiving mechanical ventilation with sepsis [5]. ΔPP has also been shown to be useful in predicting and assessing the hemodynamic effect of positive-end-expiratory pressure and fluid loading in ventilated patients with acute lung injury (ALI) [6].

The standard method for calculating ΔPP requires simultaneous recording of arterial and airway pressure. Pulse pressure (PP) is calculated on a beat-to-beat basis as the difference between systolic and diastolic arterial pressure. Maximal PP ($\mathrm{PP}_{\max}$) and minimal PP ($\mathrm{PP}_{\min}$) are calculated over a single respiratory cycle, which is determined from the airway pressure signal. Pulse pressure variations ΔPP are calculated in terms of $\mathrm{PP}_{\max}$ and $\mathrm{PP}_{\min}$ and expressed as a percentage

$$\Delta\mathrm{PP}(\%) = 100 \times \frac{\mathrm{PP}_{\max} - \mathrm{PP}_{\min}}{\frac{(\mathrm{PP}_{\max}+\mathrm{PP}_{\min})}{2}}. \quad (1)$$

Manuscript received August 27, 2003; revised March 6, 2004. This work was supported in part by the Northwest Health Foundation and in part by the Doernbecher Children's Hospital Foundation. *Asterisk indicates corresponding author*.

*M. Aboy is with the Biomedical Signal Processing Laboratory, Department of Electrical and Computer Engineering at Portland State University, 1900 SW 4th Ave., Portland, OR 97201 USA (e-mail: mateoaboy@ieee.org).

J. McNames is with the Biomedical Signal Processing Laboratory, Department of Electrical and Computer Engineering at Portland State University, Portland, OR 97201 USA.

T. Thong is with the Department of Biomedical Engineering, OGI School of Science and Engineering at Oregon Health and Science University, Portland, OR 97206 USA.

C. R. Phillips is with the Pulmonary and Critical Care Medicine Department, Oregon Health and Science University, Portland, OR 97201 USA.

M. S. Ellenby and B. Goldstein are with the Complex Systems Laboratory in the Department of Pediatrics at Oregon Health and Science University, Portland, OR 97201 USA.

Digital Object Identifier 10.1109/TBME.2004.834295

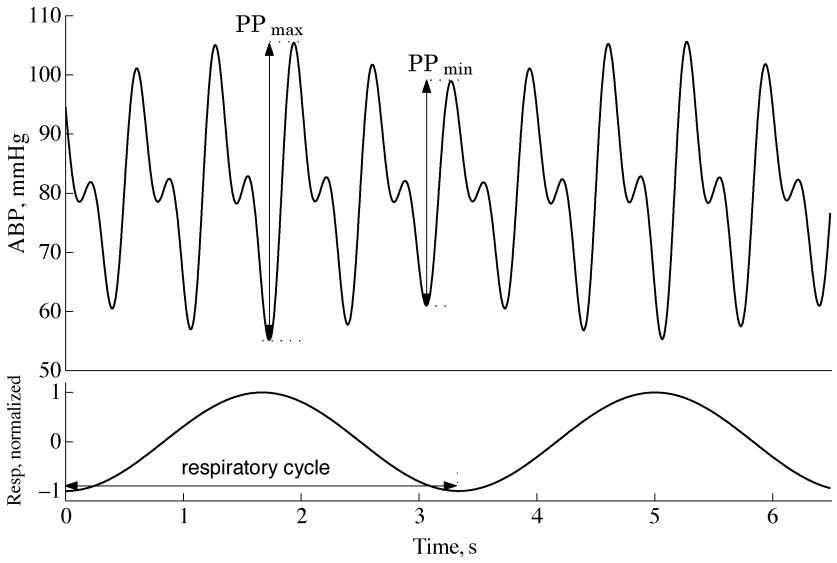

Fig. 1. Illustration of $\mathbf{PP}_{\max}$ and $\mathbf{PP}_{\min}$ during two respiratory cycles of ABP (synthetic).

Fig. 1 shows a plot of an ABP signal versus time during six heartbeats illustrating the $\mathrm{PP}_{\max}$ and $\mathrm{PP}_{\min}$ metrics used in the calculation of $\Delta\mathrm{PP}$.

We present a new algorithm to estimate $\Delta\mathrm{PP}$, and an evaluation of its performance with respect to the standard technique for calculating $\Delta\mathrm{PP}$. Our proposed methodology can be used to estimate $\Delta\mathrm{PP}$ from the ABP signal alone, eliminating the need for simultaneously acquiring airway pressure.

II. Methodology

Step 1) Beat Minima Detection: An automatic beat detection algorithm is used to detect each ABP beat. The algorithm performs minima detection to identify the time location corresponding to the start of each beat a_k

$$\boldsymbol{a} = (a_1\ a_2,\ \ldots,\ a_{k-1}\ a_k\ a_{k+1},\ \ldots)^T. \tag{2}$$

Beat detection is performed as follows: the pressure signal is preprocessed by three bandpass elliptic filters with different cutoff frequencies: 1) The output of the first bandpass filter is used to estimate the heart rate based on the estimated power spectral density (PSD). 2) The estimated heart rate is then used to calculate the cutoff frequencies of the other two filters. 3) Peak detection and decision logic is performed based on rank-order (percentile-based) nonlinear filters that incorporate relative amplitude and slope information to coarsely estimate the minima preceding each beat (a_k). 4) A nearest-neighbor algorithm is used to combine the information extracted from the relative amplitude and slope. Finally, 5) an interbeat-interval stage uses this classification together with the estimated heart rate to make the final classification and detection of signal components. Since detection is made on the filtered signal, a second nearest neighbor algorithm is used to find the minima in the raw signal that are closest to the detected components. A more detailed description of a similar algorithm for detection of systolic (ABP) and percussion (ICP) peaks is described in [7]. In principle, however, any reliable automatic beat detection algorithm could be used in this step.

Step 2) Beat Maxima Detection: The algorithm searches for the maximum in each beat b_k, using the $\boldsymbol{a}$ components identified by the beat detection algorithm in the previous step

$$b_k \triangleq \arg \max_{a_k \le n \le a_{k+1}} x(n) \tag{3}$$

$$\boldsymbol{b} = (b_1\ b_2,\ \ldots\ ,b_{k-1}\ b_k\ b_{k+1},\ \ldots)^T \tag{4}$$

where $x(n)$ denotes the ABP signal sampled at an arbitrary sampling rate f_s which satisfies the sampling theorem.

Step 3) Beat Mean Calculation: The beat mean pressure $\bar{x}_k$ is calculated by

$$\bar{x}_k \triangleq \frac{1}{a_{k+1} - a_k + 1} \sum_{k=a_k}^{a_{k+1}} x(k) \tag{5}$$

$$\bar{\boldsymbol{x}} = (\bar{x}_1\ \bar{x}_2,\ \ldots,\ \bar{x}_{k-1}\ \bar{x}_k\ \bar{x}_{k+1},\ \ldots)^T. \tag{6}$$

The beat mean pressure $\bar{x}_k$ is used as an estimate of the additive effect of respiration on ABP.

Step 4) Pulse Amplitude Pressure: The pulse amplitude pressure p_k is estimated by

$$p_k \triangleq x(b_k) - x(a_k) \tag{7}$$

$$\boldsymbol{p} = (p_1\ p_2,\ \ldots,\ p_{k-1}\ p_k\ p_{k+1},\ \ldots)^T. \tag{8}$$

The pulse amplitude p_k estimated in this step for each beat is used to validate the pulse amplitude estimated in Step 6) for each sample. It is also used to estimate dPP using standard methodology.

Fig. 2 illustrates the first four steps in a synthetic ABP signal.

Step 5) Envelope Estimation: The upper $u_e(n)$ and lower $l_e(n)$ envelopes are estimated from the $x(\boldsymbol{a})$ and $x(\boldsymbol{b})$ time series, respectively; by smoothing and uniformly resampling $x(\boldsymbol{a})$ and $x(\boldsymbol{b})$ at a rate of f_s (sampling frequency of ABP) with a kernel smoother

$$d(k) = \frac{\sum_{n=1}^{N} \delta(n) b\left(\frac{|kT_s - t(n)|}{\sigma_b}\right)}{\sum_{n=1}^{N} b\left(\frac{|kT_s - t(n)|}{\sigma_b}\right)} \tag{9}$$

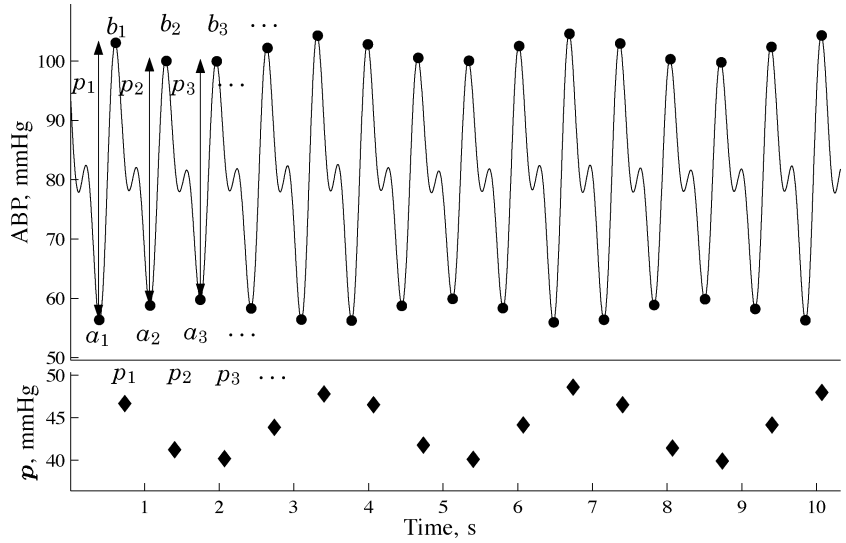

Fig. 2. Plot of an ABP signal over a 10-s period illustrating beat minima detection, beat maxima detection, and pulse amplitude pressure calculation.

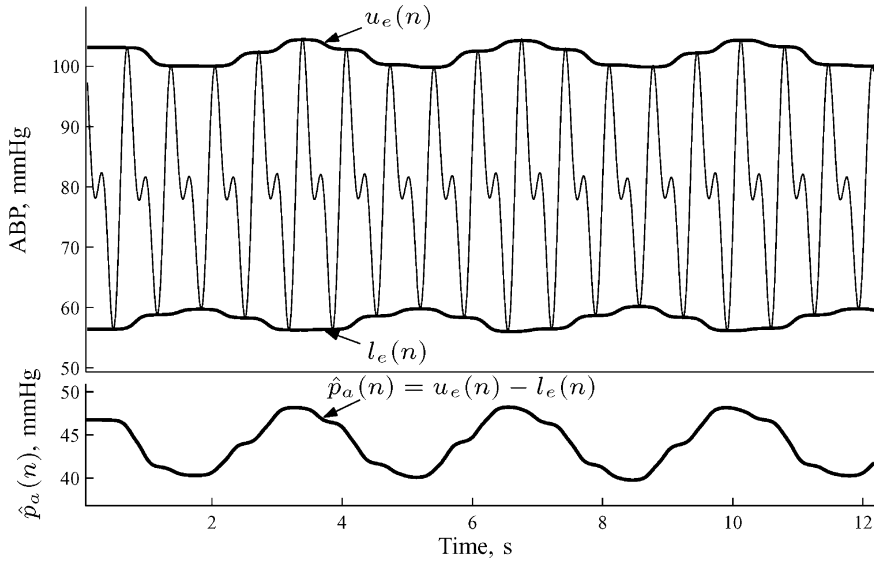

Fig. 3. Plot of an ABP signal over a 12-s period illustrating (top) envelope estimation, and (bottom) pulse amplitude pressure estimation.

where $T_s = (1/f_s)$ is the resampling interval, σ_b is the kernel width, and $b(\cdot)$ is a clipped Gaussian kernel function

$$b(u) = \begin{cases} \exp\left(\frac{-u^2}{2}\right) & \text{if } -5 \le u \le 5 \\ 0 & \text{otherwise.} \end{cases} \quad (10)$$

The kernel width is a user specified parameter that controls the degree of smoothing and depends of the fundamental frequency of the ABP signal (heart rate). A width of 0.2 s works well for human heart rates.

Step 6) Pulse Amplitude Pressure Estimation: In Step 4), we obtain an estimate of the pulse amplitude for each beat. Using the estimated $u_e(n)$ and $l_e(n)$ we can obtain an estimate of the pulse pressure for each sample of ABP according to

$$\hat{p}_a(n) \triangleq u_e(n) - l_e(n) \quad (11)$$

where $\hat{p}_a(n)$ denotes the sample-by-sample difference of $u_e(n)$ and $l_e(n)$. Fig. 3 illustrates steps 5) and 6).

Step 7) Pulse Pressure Variation Estimation: The pulse pressure variation index $\Delta\mathrm{PP}$ is estimated from the $\hat{p}_a(n)$ time series. The pulse amplitude pressure signal is low-pass filtered with a noncausal elliptic filter with $1.75 f_r$ Hz as the cutoff frequency. The respiratory frequency f_r is estimated from u_e (the fundamental frequency of u_e is an estimate of f_r.) Minima $\boldsymbol{a}_p$ and maxima $\boldsymbol{b}_p$ detection are performed on this signal to estimate the maximum $\widehat{\mathbf{PP}}_{\max}$ and minimum pulse pressures $\widehat{\mathbf{PP}}_{\min}$ over each respiratory cycle as

$$\widehat{\mathbf{PP}}_{\max} = \hat{p}_a(\boldsymbol{b}_p) \quad (12)$$

$$\widehat{\mathbf{PP}}_{\min} = \hat{p}_a(\boldsymbol{a}_p). \quad (13)$$

Based on these estimates we obtain the pulse amplitude variation $\Delta\mathrm{PP}$ according to (14)

$$\Delta\widehat{\mathbf{PP}} = \mathcal{F}_{\mathrm{med}}\left(\frac{\widehat{\mathbf{PP}}_{\max} - \widehat{\mathbf{PP}}_{\min}}{\mu}, w_l\right) \quad (14)$$

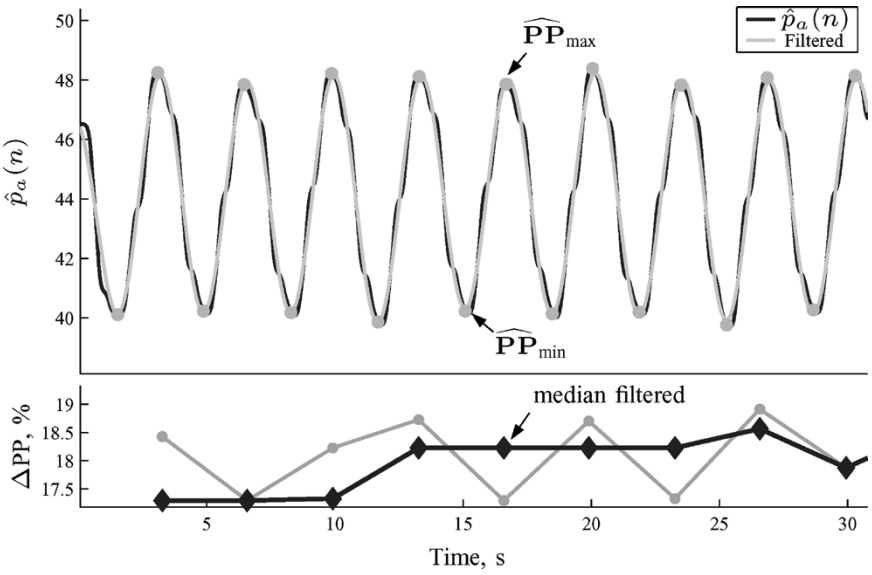

Fig. 4. Plot of an ABP signal over a 30-s period illustrating pulse pressure variation estimation.

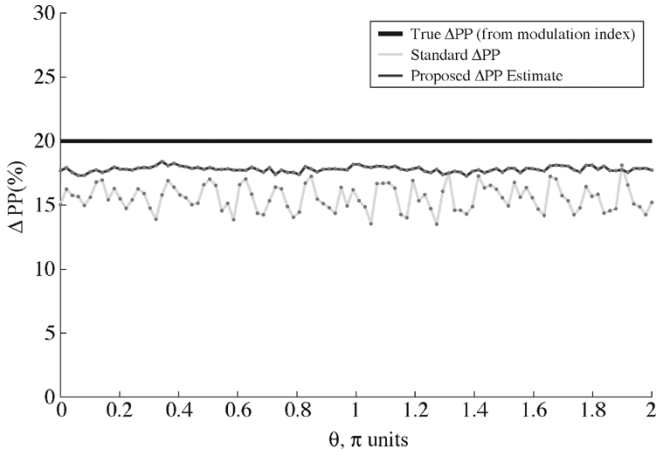

Fig. 5. Results of the simulation study comparing the proposed methodology and the standard method for estimating $\mathbf{\Delta PP}$ as the phase $\boldsymbol{\theta}$ was linearly increased from 0 to $\mathbf{2\pi}$. The true $\mathbf{\Delta PP}$ was determined from the modulation index $\boldsymbol{a}$ used in the generation the synthetic signals.

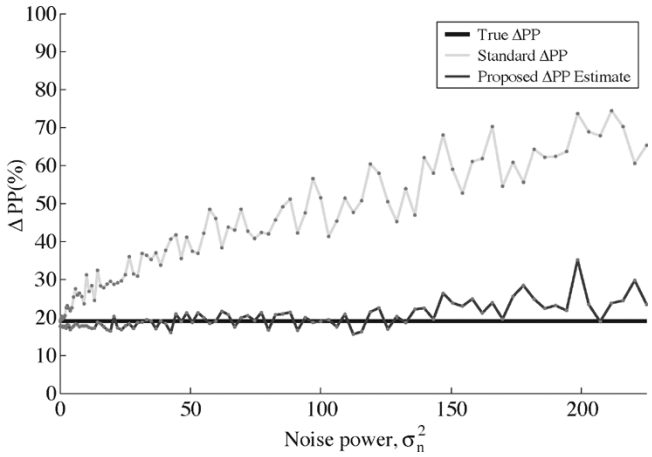

Fig. 6. Results of the simulation study comparing the proposed methodology and the standard method for estimating $\mathbf{\Delta PP}$ as a function of noise power to assess their robustness to beat misdetections.

and $\mathcal{F}_{\text{med}}(\cdot, w_l)$where μ is the mean over the respiratory cycle

$$\mu = \frac{1}{a_{p_{k+1}} - a_{p_k} + 1} \sum_{k=a_{p_k}}^{a_{p_{k+1}}} \hat{p}_a(n) \tag{15}$$

is a median filter with a window length of w_l samples. The length of the window w_l is a user specified parameter that controls the tradeoff between time resolution and robustness to noise of the estimates. Longer windows result in estimates more robust to noise but with less time resolution. Window lengths of 3–11 samples are adequate for most situations. Fig. 4 illustrates this step on an ABP signal of 30-s duration and w_l equal to 5 samples.

III. Simulation Study

In order to assess the performance of the proposed methodology, we performed the following simulation studies. In all the simulations we set w_l equal to 3 samples. The standard $\Delta\mathrm{PP}$ estimate was determined according to the procedure stated in the Introduction section. The estimates over three respiratory cycles were averaged to produce a single $\Delta\mathrm{PP}$ (often done in practice).

A. Comparison of the Proposed Estimator and the Standard $\Delta\mathrm{PP}$ as Estimates of the Respiratory Modulation Index and Their Robustness to Changes in Respiratory Phase

$\Delta\mathrm{PP}$ measures the pulse pressure variation of ABP with respiration, which is the amplitude modulation (AM) effect of the respiratory signal on ABP. As such, $\Delta\mathrm{PP}$ is an estimate of the modulation index. In this simulation we used the following model of ABP, and compared the proposed and standard $\Delta\mathrm{PP}$ estimates as estimators of the AM index a

$$\begin{aligned} p(t) &= \mu_p + [1 + a r_n(t)] \cdot [\alpha \cos 2\pi f_c t + \beta \cos(4\pi f_c t + \theta_c)] \\ r_n(t) &= \cos(2\pi f_r t + \theta) \end{aligned} \tag{16}$$

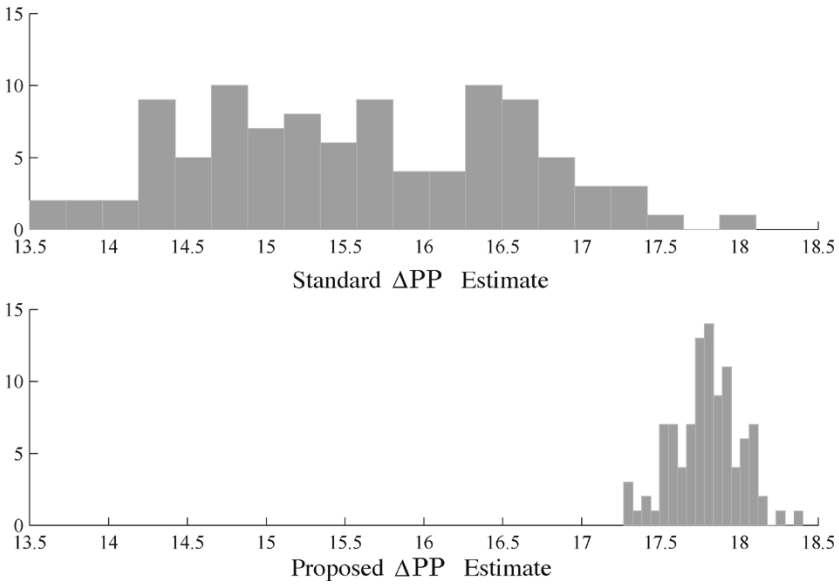

Fig. 7. Histograms of the standard $\mathbf{\Delta PP}$ and the proposed $\mathbf{\Delta PP}$ estimates obtained from the simulation study assessing their consistency when the phase of the respiratory signal $\boldsymbol{\theta}$ is linearly increased from 0 to $\boldsymbol{2\pi}$. The true $\mathbf{\Delta PP}$ (defined in terms of the modulation index) is 20.

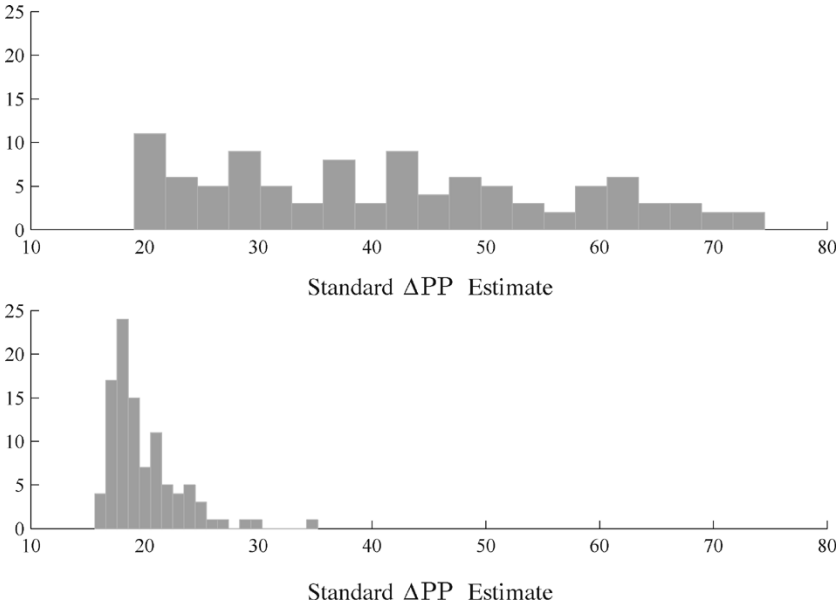

Fig. 8. Histograms of the standard $\mathbf{\Delta PP}$ and the proposed $\mathbf{\Delta PP}$ estimate obtained from the simulation study assessing their robustness to beat misdetections caused by low SNR. The true $\mathbf{\Delta PP}$ is 20.

where $p(t)$ denotes the ABP waveform, μ_p is the mean ABP pressure, a is the modulation index (AM), $r_n(t)$ is the normalized respiratory signal (modulating signal with frequency f_r), and $c(t) = \alpha \cos 2\pi f_c t + \beta \cos(4\pi f_c t + \theta))$ are the first two harmonics of the ABP signal at the cardiac frequency, f_c (carrier frequency).

We kept the modulation index constant and changed the phase θ of the respiratory signal, which should result in a constant $\Delta\mathrm{PP}$ estimate. We generated 100 ABP signals with constant modulation index $a = 0.1 = 10\%$ (this should result in a $\Delta\mathrm{PP} = 2a = 20\%$). The phase θ was linearly increased from 0 to 2π. $\Delta\mathrm{PP}$ was estimated using the standard and proposed methodologies.

B. Comparison of the Proposed Estimator and the Standard $\Delta\mathrm{PP}$ *as Function of Noise Power to Assess Their Robustness to Beat Misdetections*

This simulation assessed how robust each method is to beat misdetections. We generated an ensemble of 100 synthetic ABP signals of 60-s duration using the ABP simulator described before. We chose a constant modulation index $a = 0.1 = 10\%$ (this should result in a $\Delta\mathrm{PP} = 2a = 20\%$). The noise power was linearly increased from 0 ($\mathrm{SNR} = \infty$ dB) to 225 ($\mathrm{SNR} \approx 0$ dB). For each 60-s signal $\Delta\mathrm{PP}$ was calculated using the standard method and the new

methodology we proposed in this paper. The gold standard was defined as ΔPP calculated according to the standard definition for the ABP signal without noise. The study compared the two methods as a function of the SNR. In calculating ΔPP using the standard methodology, the ABP and respiratory signals were used. Gaussian noise was only added to the ABP signal and not to respiration. In order to eliminate the confounding factor of pulse pressure variations with noise, the noisy ABP signals were only used for beat detection (the same algorithm was used for both methods), ΔPP estimation was performed on the uncorrupted ABP signal but using the beat detections obtained from the corrupted ABP.

IV. Results and Discussion

Fig. 5 shows the simulation results comparing the standard and the proposed methodology as estimates of the respiratory modulation index (AM). The instantaneous estimates during the 60 s. of ABP were averaged for a given realization to produce an overall estimate of ΔPP for the 60 s. Each ΔPP estimate shown in this figure is the ensemble mean of the individual ΔPP estimated from each of the 100 synthetic ABP signals. The plot shows that both methods underestimate the true ΔPP but the proposed methodology shows a superior statistical performance since it is less biased and has less variance. These results also indicate that the proposed methodology is less dependent on respiratory phase shifts.

Fig. 6 shows the results of the simulation comparing the standard and proposed methodologies for ΔPP estimation. In the absence of noise (high SNR) both methods provide a similar estimate and are close to the true ΔPP. However, for low SNR resulting in beat misdetections, the proposed methodology exhibits a better performance even though it is obtained using only the corrupted ABP signal (the standard method was based on corrupted ABP and clean respiration). Fig. 7 and 8 show the histograms of the standard and proposed methodologies for ΔPP estimation for the two simulation studies. Based on these histograms we conclude that our new estimate of ΔPP is less biased and has less variance than the standard estimate. The results may differ in real ABP data due to the effects not accounted in the model. We are currently in the process of applying our algorithm to real ABP for determining ΔPP, and comparing its estimates against the standard method and the estimates obtained using commercial systems with proprietary algorithms.

V. Summary

We described a new algorithm to estimate ΔPP based on the ABP signal alone, which eliminates the need of simultaneous recording of airway pressure. Preliminary results based on validation of the algorithm with synthetic data indicate the proposed methodology is less dependent on respiratory phase shifts, is more robust to beat misdetections, is a better estimate of the true ΔPP (obtained from the AM modulation index), and has better statistical properties.

References

[1] K. Bendjelid and J. Romand, "Fluid responsiviness in mechanically ventilated patients: a review of indices used in intensive care," *Intensive Care Med*, vol. 29, pp. 352–360, 2003.

[2] F. Michard and J. Tebould, *Respiratory Changes in Arterial Pressure in Mechanically Ventilated Patients*, J. Vincent, Ed. Berlin, Germany: Springer-Verlag, 2000.

[3] A. Parry-Jones and J. Pittman, "Arterial pressure and stroke volume variability as measurements for cardiovascular optimization (review)," *Int. J. Intensive Care*, Summer 2003.

[4] F. Michard, D. Boussat, D. Chemla, and N. Anguel, "Relation between respiratory changes in arterial pulse pressure and fluid responsiveness in septic patients with acute circulatory failure," *Amer. J. Respir. Crit. Care Med.*, vol. 162, pp. 134–138, 2000.

[5] F. Michard and J.-L. Teboul, "Predicting fluid responsiveness in icu patients. A critical analysis of the evidence," *CHEST. Crit. Care Rev.*, vol. 121, pp. 2000–2008, 2002.

[6] F. Michard, D. Chemla, and C. Richard, "Clinical use of respiratory changes in arterial pulse pressure to monitor the hemodynamic effects of peep," *Amer. J. Respir. Crit. Care Med.*, vol. 159, pp. 935–939, 1998.

[7] M. Aboy, J. McNames, and B. Goldstein, "Automatic detection algorithm of intracranial pressure waveform components," in *Prot. 23th Int. Conf. IEEE Engineering in Medicine and Biology Society, 2001*, vol. 3, Oct. 2001, pp. 2231–2234.

A Refined Bootstrap Method for Estimating the Zernike Polynomial Model Order for Corneal Surfaces

D. Robert Iskander*, Mark R. Morelande, Michael J. Collins, and Tobias Buehren

***Abstract*—Following our previous work on optimal modeling of corneal surfaces with Zernike polynomials, we have developed a refined bootstrap-based procedure which improves the accuracy of the previous method. We show that for normal corneas, the optimal number of Zernike terms usually corresponds to the fourth or fifth radial order expansion of Zernike polynomials. On the other hand, for distorted corneas such as those encountered in keratoconus or in surgically altered cases, the estimated model was found to be up to three radial orders higher than for normal corneas.**

***Index Terms*—Cornea, model order selection, resampling techniques.**

I. Introduction

Modeling corneal surfaces with Zernike polynomials often leads to the question of the number of Zernike terms that should be used [1]. Recently, we have developed a bootstrap-based method to perform this task [2]. We have shown in simulations that the bootstrap method outperforms the classical model order selection techniques under the assumption that the measurement noise is independent and identically distributed (i.i.d.) across the whole corneal surface. In a further study [3], we have shown that this technique is appropriate in the context of fitting Zernike polynomials to corneal elevation data of normal subjects (i.e. subjects with healthy corneas), allowing judicious selection of the optimal number of Zernike terms.

Manuscript received October 24, 2002; revised March 6, 2004. *Asterisk indicates corresponding author*.

*D. R. Iskander is with the Contact Lens and Visual Optics Laboratory, School of Optometry, Queensland University of Technology, Victoria Park Rd, Kelvin Grove Q4059, Australia (e-mail: d.iskander@qut.edu.au).

M. R. Morelande is with the CRC for Sensor Signal and Information Processing, Department of Electrical and Electronic Engineering, The University of Melbourne, Parkville VIC 3010, Australia (e-mail: m.morelande@ee.mu.oz.au).

M. J. Collins and T. Buehren are with the Contact Lens and Visual Optics Laboratory, School of Optometry, Queensland University of Technology, Kelvin Grove Q4059, Australia (e-mail: m.collins@qut.edu.au; t.buehren@qut.edu.au).

Digital Object Identifier 10.1109/TBME.2004.834252